

3DRISM Multigrid Algorithm for Fast Solvation Free Energy Calculations

Volodymyr P. Sergiievskyi[†] and Maxim V. Fedorov^{*,‡}

[†]Max Planck Institute for Mathematics in the Sciences, Inselstrasse 22, 04103 Leipzig, Germany

[‡]Nanoscience Division, Department of Physics, Scottish Universities Physics Alliance (SUPA), Strathclyde University, Room JA 6.10, John Anderson Building 107, Rottenrow East Glasgow, United Kingdom G4 0NG

S Supporting Information

ABSTRACT: In this paper we present a fast and accurate method for modeling solvation properties of organic molecules in water with a main focus on predicting solvation (hydration) free energies of small organic compounds. The method is based on a combination of (i) a molecular theory, three-dimensional reference interaction sites model (3DRISM); (ii) a fast multigrid algorithm for solving the high-dimensional 3DRISM integral equations; and (iii) a recently introduced universal correction (UC) for the 3DRISM solvation free energies by properly scaled molecular partial volume (3DRISM-UC, Palmer et al., *J. Phys.: Condens. Matter* **2010**, 22, 492101). A fast multigrid algorithm is the core of the method because it helps to reduce the high computational costs associated with solving the 3DRISM equations. To facilitate future applications of the method, we performed benchmarking of the algorithm on a set of several model solutes in order to find optimal grid parameters and to test the performance and accuracy of the algorithm. We have shown that the proposed new multigrid algorithm is on average 24 times faster than the simple Picard method and at least 3.5 times faster than the MDIIS method which is currently actively used by the 3DRISM community (e.g., the MDIIS method has been recently implemented in a new 3DRISM implicit solvent routine in the recent release of the AmberTools 1.4 molecular modeling package (Luchko et al. *J. Chem. Theory Comput.* **2010**, 6, 607–624). Then we have benchmarked the multigrid algorithm with chosen optimal parameters on a set of 99 organic compounds. We show that average computational time required for one 3DRISM calculation is 3.5 min per a small organic molecule (10–20 atoms) on a standard personal computer. We also benchmarked predicted solvation free energy values for all of the compounds in the set against the corresponding experimental data. We show that by using the proposed multigrid algorithm and the 3DRISM-UC model, it is possible to obtain good correlation between calculated and experimental results for solvation free energies of aqueous solutions of small organic compounds (correlation coefficient 0.97, root-mean-square deviation <1 kcal/mol).

INTRODUCTION

Integral equation theory of liquids (IETL) is a useful method for theoretical studies of structural and thermodynamical properties of liquids. IETL describes the liquid structure in terms of correlation functions. The central equation in IETL is the Ornstein–Zernike (OZ) equation.¹ In its general molecular form this equation operates with six-dimensional correlation functions even in the case of isotropic molecular systems.² Because of the high computational complexity, an efficient numerical solution of the high-dimensional molecular OZ equation is still an open problem. Therefore, there have been developed some approximate models that help to reduce dimensionality of integral equations. The most popular model in this field is the reference interaction site model (RISM).³ One of the main approximations behind the original RISM model is that the high-dimensional molecular correlation functions are represented by a set of spherically symmetric site–site functions. That approximation reduces the original high-dimensional problem to a set of (technically) one-dimensional equations. Due to this fact, the RISM theory is also referenced as 1DRISM.

From a computational point of view, it is relatively inexpensive to solve the 1DRISM equations numerically for small molecular solutes (<10² atoms) with modern computers,

and typically, solutions of the 1DRISM equations give a qualitatively correct description of the solvent structure around the solute. To compare, it was shown that RISM solvent representation is more accurate than continuum solvent representation in continuum electrostatics models.^{4–6} In addition, RISM theory gives end-point expressions for solvation free energy (SFE) that avoid thermodynamical integration.^{7,8} We note though that the original formulas for SFE calculations^{7,8} provide only qualitative predictions of trends in the differences of SFEs for different compounds.⁹ Recently there were proposed several methods for parametrizing RISM SFE calculations that predict SFEs with an accuracy around 1 kcal/mol.^{9–13} However, decomposition of molecular functions to site–site spherically symmetric functions leads to inaccurate representation of molecular structure. Therefore, a considerable number of empirical corrections is necessary to achieve good accuracy of predictions.

Another approximation of the OZ equation is the so-called three-dimensional RISM (3DRISM),^{14,15} where a solute molecule is represented as a three-dimensional object. The 3DRISM operates with a set of three-dimensional equations

Received: November 14, 2011

Published: April 13, 2012



and provides better spatial description of solute–solvent correlations than the 1DRISM. The 3DRISM method is currently widely used in biochemical applications for the description of solvation properties of biomolecules.^{16–19} Another promising application of the 3DRISM theory is computational screening of large databases of drug candidates. As it was recently shown, a 3DRISM-based method accurately predicts thermodynamic parameters of hydrated organic molecules including drug-like molecules.^{20,21} However, for small molecules, numerical solution of the multidimensional 3DRISM equations requires significantly more computational time than solution of the 1DRISM equations.²¹ High computational expenses of 3DRISM calculations is a real bottleneck of this method that inhibits wider applications of this technique. In the current work, we show that this problem can be overcome by using of highly efficient multigrid algorithms.

Coming back to the history of the IETL, the first algorithm used for solving OZ-like integral equations was presumably the Picard iteration method.²² This method is easy to implement. However, it has a comparably low-convergence rate. Therefore, there were proposed several alternative iteration schemes in order to improve the convergence rate, such as the Newton–Raphson method (NR),²³ the NR-generalized minimal residual method (NR-GMRES) algorithm,²⁴ the combined NR-direct inversion in iterative subspace (NR-DIIS) iteration,²⁵ the modified DIIS (MDIIS) method,²⁶ and the vector extrapolation method.²⁷ Recently an efficient 3DRISM equations solver which uses the MDIIS algorithm was implemented in the Amber molecular modeling software.¹⁸

Another way to increase the speed of calculations is to use two- and multiscale methods.^{28–30} However, from a mathematical point of view it is necessary to use all advantages of the multiscale approach. From the applied mathematics perspective, there is a general ‘multigrid’ (MG) technique that is well investigated theoretically and is rigorously proven to be effective.³⁵ These days the multigrid technique is widely used in several areas of computational chemistry (particularly in quantum chemistry and material sciences).^{36–39} In spite of this, only recently the multigrid methods attracted attention of the RISM community.^{40–42} In our recent work we have shown that the multigrid technique allows one to increase the performance of the numerical 1DRISM solver up to a dozen times.⁴² One of the main goals of the current work is to develop a fast algorithm for solving the 3DRISM equations, because the latter have been proven to be more advanced from a theoretical point of view.^{21,43–47}

We note that general theoretical framework of the multigrid method for solving RISM equations, proposed in ref 42, allows one to combine this method with other different numerical solvers. In our work we investigate the numerical performance of two modifications of the multigrid 3DRISM algorithm where the multigrid is combined with (i) the Picard iteration method (MG-Picard) and (ii) with the MDIIS method (MG-MDIIS), respectively. By benchmarking of these methods on a set of model compounds, we determine the optimal grid parameters for solvation (hydration) free energy calculations. We test the numerical performance of the proposed methods and compare it to the performance of the standard Picard iteration and MDIIS methods. Additionally, we benchmark the speed and accuracy of the algorithm on an extended set of 99 organic compounds. First, we test computational performance of the algorithm and then test the accuracy of the SFE calculations

with the universal correction (UC) model, as proposed in ref 10. To check the accuracy of the free energy results, we calculate the correlation coefficient and the root-mean-square deviation between calculated and experimental data.

METHOD

3D RISM. In our work we use the Kovalenko-Hirata formulation of the 3D RISM theory^{44,48} in order to describe infinitely diluted solutions of small organic solute molecules. Solvent (water) molecules are described by the 1DRISM approximation, while a solute molecule is a three-dimensional object. Structure of the solvent is described by the total and direct correlation functions $h_\alpha(\mathbf{r})$, $c_\alpha(\mathbf{r})$ where α indicates a solvent site. The 3DRISM equations are written in the following way:

$$h_\alpha(\mathbf{r}) = \sum_{\xi=1}^{N_{\text{solvent}}} \int_{\mathbb{R}^3} c_\xi(\mathbf{r}' - \mathbf{r}) \chi_{\xi\alpha}(\mathbf{r}') d\mathbf{r}' \quad (1)$$

where N_{solvent} is the number of solvent sites, $\chi_{\xi\alpha}(\mathbf{r})$ is the solvent susceptibility function for sites ξ and α . Solvent susceptibility functions $\chi_{\xi\alpha}(\mathbf{r})$ are defined as following:

$$\chi_{\xi\alpha}(\mathbf{r}) = \omega_{\xi\alpha}(r) + \rho h_{\xi\alpha}^{\text{sol}}(r) \quad (2)$$

where $r = |\mathbf{r}|$, $\omega_{\xi\alpha}(r) = \delta_{\xi\alpha} + (1 - \delta_{\xi\alpha})\delta(r - r_{\xi\alpha})/(4\pi r_{\xi\alpha}^2)$, $r_{\xi\alpha}$ is the distance between the sites ξ and α of a solvent molecule, $h_{\xi\alpha}^{\text{sol}}(r)$ is the total site–site correlation function of the solvent sites ξ and α , $\delta_{\xi\alpha}$ is the Kronecker delta, and $\delta(r)$ is the Dirac delta function. In this paper we used the functions $h_{\xi\alpha}^{\text{sol}}(r)$ calculated in ref 49.

Equation 1 is completed by closure relations:

$$h_\alpha(\mathbf{r}) = e^{-\beta U_\alpha(r) + h_\alpha(\mathbf{r}) - c_\alpha(\mathbf{r}) + B_\alpha(\mathbf{r})} - 1 \quad (3)$$

where $\beta = 1/k_B T$, k_B is the Boltzmann constant, T is the temperature, $U_\alpha(\mathbf{r})$ is the interaction potential corresponding to a solute site α , and $B_\alpha(\mathbf{r})$ is the bridge functional.

To use iterative solvers we rewrite the eq 1 in the following form:⁵⁰

$$\gamma_\alpha(\mathbf{r}) = \sum_{\xi=1}^{N_{\text{solvent}}} \int_{\mathbb{R}^3} C[\gamma_\xi(\mathbf{r}' - \mathbf{r})] \chi_{\xi\alpha}(\mathbf{r}') d\mathbf{r}' + \theta_\alpha(\mathbf{r}) - C[\gamma_\alpha(\mathbf{r})] \quad (4)$$

where $\gamma_\alpha(\mathbf{r}) = h_\alpha(\mathbf{r}) - c_\alpha^S(\mathbf{r})$, $c_\alpha^S(\mathbf{r}) = c_\alpha(\mathbf{r}) + \beta U_\alpha^L(\mathbf{r})$, $U_\alpha(\mathbf{r}) = U_\alpha^S(\mathbf{r}) + U_\alpha^L(\mathbf{r})$, $U_\alpha^S(\mathbf{r})$ is a short-range potential, $U_\alpha^L(\mathbf{r})$ is a long-range potential, $\theta_\alpha(\mathbf{r}) = -\beta \sum_\xi \int_{\mathbb{R}^3} U_\xi^L(\mathbf{r}' - \mathbf{r}) \chi_{\xi\alpha}(\mathbf{r}') d\mathbf{r}'$, $C[\cdot]$ is a closure (bridge) functional.

We use interaction potentials which are superpositions of the site–site interaction potentials:

$$U_\alpha^S(\mathbf{r}) = \sum_{s=1}^{N_{\text{solute}}} u_{s\alpha}^S(|\mathbf{r} - \mathbf{r}_s|) \quad (5)$$

$$U_\alpha^L(\mathbf{r}) = \sum_{s=1}^{N_{\text{solute}}} u_{s\alpha}^L(|\mathbf{r} - \mathbf{r}_s|) \quad (6)$$

where \mathbf{r}_s is the position of a solute site s with respect to the center of a molecule and N_{solute} is the number of solute sites. In our work the site–site potentials contain Lennard-Jones (LJ) and Coulomb parts. Pair LJ parameters are obtained from the

atomic LJ parameters by using the Lorentz–Berthelot mixing rules:

$$\sigma_{sa} = \frac{1}{2}(\sigma_s + \sigma_a) \quad \varepsilon_{sa} = \sqrt{\varepsilon_s \varepsilon_a} \quad (7)$$

To avoid divergence of the algorithm due to the long-range behavior of the interaction potentials, we separate the short- and long-ranges of the potentials and then treat them separately by using the Ng procedure.⁵¹ We use the atomic units for distance and energy Bohr = 0.52918×10^{-10} m and Hartree = $4.35974394 \times 10^{18}$ J. This allows us to avoid scaling coefficients in the representation of the Coulomb potential. Thus expressions for the short- and long-range potentials are written as follows:

$$u_{sa}^S(r) = u_{sa}^{\text{LJ}(\text{short})}(r) + u_{sa}^C(r)(1 - \text{erf}(\tau r)) \quad (8)$$

$$u_{sa}^L(r) = u_{sa}^{\text{LJ}(\text{long})}(r) + u_{sa}^C(r)\text{erf}(\tau r) \quad (9)$$

where $u_{sa}^C(r)$ is the Coulomb component of the site–site potential, $\text{erf}(r) = \int_{-\infty}^r e^{-t^2} dt$, $\tau = 0.5 \text{ Bohr}^{-1}$, $u_{sa}^{\text{LJ}(\text{short})}(r)$, $u_{sa}^{\text{LJ}(\text{long})}(r)$ are short- and long-range components of the LJ potential, respectively. The latter are defined by the following relations:

$$u_{sa}^{\text{LJ}(\text{short})}(r) = \begin{cases} u_{sa}^{\text{LJ}}(r) - u_{sa}^{\text{LJ}}(R_{\text{cut}}) & \text{when } r < R_{\text{cut}} \\ 0 & \text{otherwise} \end{cases} \quad (10)$$

$$u_{sa}^{\text{LJ}(\text{long})}(r) = u_{sa}^{\text{LJ}}(r) - u_{sa}^{\text{LJ}(\text{short})}(r) \quad (11)$$

where $u_{sa}^{\text{LJ}}(r)$ is a LJ component of a site–site potential and $R_{\text{cut}} = 8 \text{ \AA}$.

In the article we use the Kovalenko–Hirata (KH) closure, which is defined as following:⁵²

$$C[\gamma_\alpha(\mathbf{r})] = \begin{cases} e^{-\beta U_\alpha^S(\mathbf{r}) + \gamma_\alpha(\mathbf{r})} - \gamma_\alpha(\mathbf{r}) - 1 & \text{when } -\beta U_\alpha^S(\mathbf{r}) + \gamma_\alpha(\mathbf{r}) > 0 \\ -\beta U_\alpha^S(\mathbf{r}) & \text{otherwise} \end{cases} \quad (12)$$

In the numerical representation of eq 4, the functions $\gamma_\alpha(\mathbf{r})$, $\chi_{\xi\alpha}(\mathbf{r})$, and $\theta_\alpha(\mathbf{r})$ are defined by their values in the grid points of an uniform Cartesian grid. A grid is defined by two parameters: spacing and buffer. Spacing is the smallest distance between the grid points, and buffer is the minimal distance from the solute atoms to the boundaries of the grid (see Figure 1 for

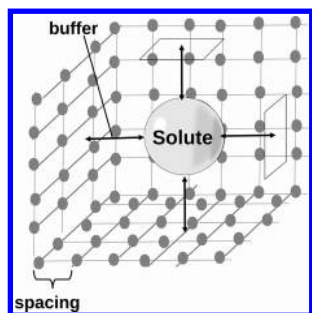


Figure 1. Spacing is the minimal distance between the grid points, and buffer is the minimal distance from the solute atoms to the boundaries of the grid.

explanations). At first glance, such parametrization may seem to be inconvenient from a theoretical point of view because the same buffer and spacing parameters may give different grids for different solutes. However, our work is mostly oriented toward future practical applications of the method, and in practical applications, we are interested in the accuracy of calculations for different cutoff distances of the correlation functions; and these cutoff distances for a Cartesian grid are defined by the buffer parameter. Using the same buffer parameter, we can adjust the size and the shape of the grid preserving a constant cutoff of the solvent correlation functions for different solutes. That provides us a straightforward way to control the accuracy of calculations.

We denote the forward and the inverse Fourier transforms on the grid \mathcal{G} as $\mathcal{F}_{\mathcal{G}}[\cdot]$, $\mathcal{F}_{\mathcal{G}}^{-1}[\cdot]$, correspondingly. Then a discrete analogue of eq 4 reads as

$$\mathbf{\Gamma}^{\mathcal{G}} = \mathcal{F}_{\mathcal{G}}^{-1}[\hat{\mathbf{X}} \cdot \mathcal{F}_{\mathcal{G}}[C[\mathbf{\Gamma}^{\mathcal{G}}]]] + \mathbf{\Theta}^{\mathcal{G}} - C[\mathbf{\Gamma}^{\mathcal{G}}] \quad (13)$$

where $\mathbf{\Gamma}^{\mathcal{G}} = (\gamma_1^{\mathcal{G}}, \dots, \gamma_{N_{\text{solvent}}}^{\mathcal{G}})^T$, $\mathbf{\Theta}^{\mathcal{G}} = (\theta_1^{\mathcal{G}}, \dots, \theta_{N_{\text{solvent}}}^{\mathcal{G}})^T$, $\hat{\mathbf{X}}^{\mathcal{G}} = [\hat{\chi}_{\xi\alpha}^{\mathcal{G}}]_{N_{\text{solvent}} \times N_{\text{solvent}}}$, $\hat{\chi}_{\xi\alpha}^{\mathcal{G}} = \mathcal{F}_{\mathcal{G}}[\chi_{\xi\alpha}^{\mathcal{G}}]$, upper index \mathcal{G} means that functions are given by their values in the grid points of the grid \mathcal{G} .

Equation 13 can be written in a more compact way:

$$\mathbf{\Gamma}^{\mathcal{G}} = F[\mathbf{\Gamma}^{\mathcal{G}}] \quad (14)$$

where $F[\mathbf{\Gamma}^{\mathcal{G}}] = \mathcal{F}_{\mathcal{G}}^{-1}[\hat{\mathbf{X}} \cdot \mathcal{F}_{\mathcal{G}}[C[\mathbf{\Gamma}^{\mathcal{G}}]]] + \mathbf{\Theta}^{\mathcal{G}} - C[\mathbf{\Gamma}^{\mathcal{G}}]$.

The Picard iteration method is defined by the following recurrent formula:

$$\mathbf{\Gamma}_{n+1}^{\mathcal{G}} = (1 - \lambda)\mathbf{\Gamma}_n^{\mathcal{G}} + \lambda F[\mathbf{\Gamma}_n^{\mathcal{G}}] \quad (15)$$

where $\mathbf{\Gamma}_n^{\mathcal{G}}$ is the n -th step approximation and λ is the coupling parameter.

DIIS and MDIIS Iteration. The direct inverse in the iterative subspace (DIIS) method is an iteration method initially introduced to improve convergence of Schrödinger equation solvers.⁵³ Later modified, the DIIS (MDIIS) method was applied to the 3DRISM equations.²⁶ In the DIIS method on the n -th iteration step one finds an approximate solution $\mathbf{\Gamma}_*^{\mathcal{G}}$ which is a linear combination of the approximations on the k previous iteration steps:

$$\mathbf{\Gamma}_*^{\mathcal{G}} = \sum_{i=1}^k c_i \mathbf{\Gamma}_{n-k+i}^{\mathcal{G}} \quad (16)$$

Below we describe the DIIS and MDIIS algorithms which solve the 3DRISM equations in the form (eq 14). We also plan to use the MDIIS algorithm in our multigrid scheme. This will require to consider a generalized task in the following form:

$$\mathbf{\Gamma}^{\mathcal{G}} = F[\mathbf{\Gamma}^{\mathcal{G}}] + \mathbf{D}^{\mathcal{G}} \quad (17)$$

where $\mathbf{D}^{\mathcal{G}} = (\mathbf{d}_1^{\mathcal{G}}, \dots, \mathbf{d}_{N_{\text{solvent}}}^{\mathcal{G}})^T$ is an arbitrary vector of corrections. The vector of corrections will be calculated during the multigrid algorithm when we move from one grid to another one. This procedure is described in the next section of the paper. In the current section we describe one-grid solvers where vector $\mathbf{D}^{\mathcal{G}}$ is given. Below we describe the DIIS and MDIIS algorithms for a general case of an arbitrary vector \mathbf{D}

having in mind that the 3DRISM equations (eq 14) correspond to the case $\mathbf{D}^{\mathcal{G}} \equiv 0$.

In the DIIS method the coefficients C_i in the eq 16 are chosen to minimize the norm of the residue $\Delta_*^{\mathcal{G}} = \Gamma_*^{\mathcal{G}} - F[\Gamma_*^{\mathcal{G}}] - \mathbf{D}^{\mathcal{G}}$. If one assumes linearity of the operator F (which for smooth operators is locally true), then the task reduces to the following system of linear equations:⁵³

$$\begin{pmatrix} a_{11} & \dots & a_{1k} & -1 \\ \vdots & \ddots & \vdots & -1 \\ a_{k1} & \dots & a_{kk} & -1 \\ 1 & \dots & 1 & 0 \end{pmatrix} \begin{pmatrix} C_1 \\ \vdots \\ C_k \\ \lambda \end{pmatrix} = \begin{pmatrix} 0 \\ \vdots \\ 0 \\ 1 \end{pmatrix} \quad (18)$$

where $a_{ij} = \int_{\mathbb{R}^3} \Delta_i(\mathbf{r}) \Delta_j(\mathbf{r}) d\mathbf{r}$, $\Gamma_{n-k+i}^{\mathcal{G}} - F[\Gamma_{n-k+i}^{\mathcal{G}}] - \mathbf{D}^{\mathcal{G}}$. In the DIIS method $\Gamma_*^{\mathcal{G}}$ is used as a solution approximation on the $(n+1)$ iteration step. However, such a procedure can lead to a linearly dependent system of equations. The MDIIS iteration method avoids this problem by adding a weighted residue to the $(n+1)$ step approximation:²⁶

$$\Gamma^{\mathcal{G}} = \Gamma_*^{\mathcal{G}} + \eta(F[\Gamma_*^{\mathcal{G}}] + \mathbf{D}^{\mathcal{G}} - \Gamma_*^{\mathcal{G}}) \quad (19)$$

where η is a weight for the residue. In combination with the standard damping technique the solution approximation on the $(n+1)$ step $\Gamma_{n+1}^{\mathcal{G}}$ in the MDIIS method can be found by using the following formula:

$$\Gamma_{n+1}^{\mathcal{G}} = (1 - \lambda)\Gamma_n^{\mathcal{G}} + \lambda\Gamma_*^{\mathcal{G}} + \lambda\eta(F[\Gamma_*^{\mathcal{G}}] + \mathbf{D}^{\mathcal{G}} - \Gamma_*^{\mathcal{G}}) \quad (20)$$

In our work we use $\lambda = 0.5$ and $\eta = 0.3$. These values are suboptimal and allow to ensure stability of the algorithm and in the same time retain reasonable performance. Detailed description of the dependence of the computation time on λ and η parameters is given in the Supporting Information to the paper.

To make notations shorter, we introduce the MDIIS operator $\Xi[\cdot, \cdot]$:

$$\Xi[\Gamma_n^{\mathcal{G}}, \mathbf{D}^{\mathcal{G}}] = (1 - \lambda)\Gamma_n^{\mathcal{G}} + \lambda\Gamma_*^{\mathcal{G}} + \lambda\eta(F[\Gamma_*^{\mathcal{G}}] + \mathbf{D}^{\mathcal{G}} - \Gamma_*^{\mathcal{G}}) \quad (21)$$

Multigrid. We use the multigrid technique in order to decrease the computation time spent on solving the 3DRISM equations. General description of the multigrid theory can be found in the book.³⁵ Here we give only short description of the multigrid method applied to the 3DRISM equations. More information on the theoretical background of the method can be found in our recent paper, where a similar computational framework for an efficient algorithm for solving the 1DRISM equations is described.⁴²

In the multigrid method the numerical task is discretized on several grids with the same buffer but different spacings. Grids with smaller numbers of points and larger spacings are called coarse grids, and grids with larger number of the points and smaller spacings are called fine grids. In our work we consider grids where number of points differ by the factor of 2^n , where $n = 0, 1, 2, \dots$

We introduce operators $p[\cdot]$ and $r[\cdot]$, which convert a coarse grid to a finer one and vice versa. We introduce an operator $R[\cdot]$, which maps a fine-grid function to a coarse grid.

$$R[\Gamma^{\mathcal{G}}] = \Gamma^{r[\mathcal{G}]} \quad (22)$$

Also we introduce an operator $P[\cdot]$, which interpolates a coarse-grid function to a fine grid:

$$P[\Gamma^{r[\mathcal{G}]}] = \Gamma^{\mathcal{G}} \quad (23)$$

In this paper we use the linear interpolation operator.

To make notations simpler, we introduce an operator $\Lambda[\cdot, \cdot]$:

$$\Lambda[\Gamma_{\mathcal{G}}; \mathbf{D}^{\mathcal{G}}] = (1 - \lambda)\Gamma^{\mathcal{G}} + \lambda(F_{\mathcal{G}}[\Gamma^{\mathcal{G}}] + \mathbf{D}^{\mathcal{G}}) \quad (24)$$

A multigrid iterative algorithm which solves the task in eq 17 can be written in the following form:

$$\Gamma_{n+1}^{\mathcal{G}} = \mathcal{M}_{\mathcal{G}}^l[\Gamma_n^{\mathcal{G}}; \mathbf{D}^{\mathcal{G}}] \quad (25)$$

where $\Gamma_n^{\mathcal{G}}$ is the n -th step approximation, $\mathcal{M}_{\mathcal{G}}^l[\cdot, \cdot]$ is a multigrid operator which performs one multigrid iteration step of the depth l on the grid \mathcal{G} . To calculate the multigrid operator of the depth $l = 0$ one performs m_0 one-grid iteration steps on the grid \mathcal{G} . The multigrid technique can be applied to both: the Picard and the MDIIS iteration methods. We define a generalized operator $\Phi[\cdot, \cdot]$ in the following way:

$$\Phi[\Gamma_n^{\mathcal{G}}; \mathbf{D}^{\mathcal{G}}] = \begin{cases} \Lambda[\Gamma_n^{\mathcal{G}}; \mathbf{D}^{\mathcal{G}}] & \text{for MG-Picard method} \\ \Xi[\Gamma_n^{\mathcal{G}}; \mathbf{D}^{\mathcal{G}}] & \text{for MG-MDIIS method} \end{cases} \quad (26)$$

Then the multigrid operator of the depth $l = 0$ is defined as

$$\mathcal{M}_{\mathcal{G}}^0[\Gamma^{\mathcal{G}}; \mathbf{D}^{\mathcal{G}}] = \Phi^{m_0}[\Gamma^{\mathcal{G}}; \mathbf{D}^{\mathcal{G}}] \quad (27)$$

For $l > 0$, given the n -th step approximation $\Gamma_n^{\mathcal{G}}$ and the correction vector $\mathbf{D}^{\mathcal{G}}$, the multigrid operator $\mathcal{M}_{\mathcal{G}}^l[\cdot, \cdot]$ is calculated by the following algorithm:

Input parameters: $\Gamma_n^{\mathcal{G}}, \mathbf{D}^{\mathcal{G}}, l$

Result: $\Gamma_{n+1}^{\mathcal{G}} = \mathcal{M}_{\mathcal{G}}^l[\Gamma_n^{\mathcal{G}}; \mathbf{D}^{\mathcal{G}}]$

- (1) Perform ν_1 Picard iteration steps on the fine grid (in our work $\nu_1 = 5$):

$$\Gamma^{r[\mathcal{G}]} = \Lambda^{\nu_1}[\Gamma_n^{\mathcal{G}}; \mathbf{D}^{\mathcal{G}}]$$

- (2) Move to the coarse grid $r[\mathcal{G}]$:

$$\Gamma_{(0)}^{r[\mathcal{G}]} = R[\Gamma^{r[\mathcal{G}]}]$$

- (3) Calculate the coarse-grid correction:

$$\mathbf{E}^{r[\mathcal{G}]} = R[F[\Gamma_{(0)}^{r[\mathcal{G}}]] - F[\Gamma_{(0)}^{r[\mathcal{G}}]]$$

- (4) Perform recursively μ multigrid iteration steps of depth $l-1$ on the coarse-grid (in our work $\mu = 1$):

$$\Gamma_{(\mu)}^{r[\mathcal{G}]} = (\mathcal{M}_{r[\mathcal{G}]}^{l-1})^{\mu}[\Gamma_{(0)}^{r[\mathcal{G}]}; R[\mathbf{D}^{\mathcal{G}}] + \mathbf{E}^{r[\mathcal{G}]}]$$

- (5) Correct the fine-grid solution using the coarse-grid results:

$$\Gamma^{r[\mathcal{G}]} = \Gamma^{r[\mathcal{G}]} + P[\Gamma_{(\mu)}^{r[\mathcal{G}]} - \Gamma_{(0)}^{r[\mathcal{G}]}]$$

- (6) Perform ν_2 Picard iteration steps on the fine grid (in our work $\nu_2 = 0$):

$$\Gamma_{n+1}^{\mathcal{G}} = \Lambda^{\nu_2}[\Gamma^{r[\mathcal{G}]}; \mathbf{D}^{\mathcal{G}}]$$

In this paper, the number of the iteration steps m_0 in the multigrid operator of the depth $l = 0$ depends on the number of the multigrid iteration step n : $m_0 = m_0(n)$. We define $m_0(n)$ in such a way that after $m_0(n)$ iteration steps, a residue decays by the factor K_n :

$$K_n \|\Phi^{m_0(n)}[\Gamma_n^{\mathcal{G}}; \mathbf{D}^{\mathcal{G}}] - \Phi^{m_0(n)+1}[\Gamma_n^{\mathcal{G}}; \mathbf{D}^{\mathcal{G}}]\| < \|\Gamma_n^{\mathcal{G}} - \Phi[\Gamma_n^{\mathcal{G}}; \mathbf{D}^{\mathcal{G}}]\| \quad (28)$$

We call the value K_n the decay factor.

Constant decay factor may lead to a nonsmooth decay of residue from one multigrid iteration step to another, which in turn leads to increasing of the number of the idle coarse-grid iteration steps (see Figure 2, solid line). To achieve a smoother

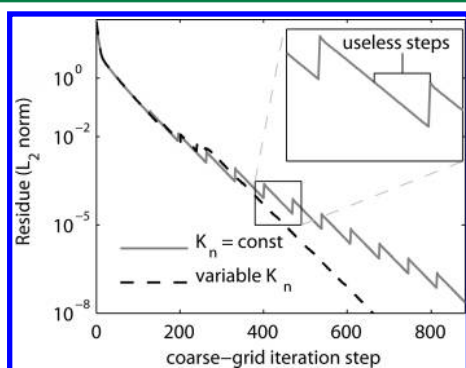


Figure 2. Coarse-grid residue decays with the number of the iteration steps in the multigrid method. Two cases are shown: constant decay factor $K_n = 10$ (solid line), and variable decay factor K_n (dashed line). System: argon aqueous solution, spacing 0.1 Å, and buffer 6.4 Å. Peaks on the saw-shaped line ($K_n = \text{const}$) correspond to the boundaries of multigrid iteration steps. The coarse-grid correction is recalculated when iteration returns from the coarse grid to the fine grid. Saw-shaped line means that iteration steps on a coarse grid are performed even after the desired accuracy of the coarse-grid correction calculation has been achieved. Thus, a significant number of coarse-grid iteration steps is actually idle because they do not improve the final result. Introducing a variable decay factor allows one to adjust the accuracy of the coarse-grid calculations and to avoid the idle iteration steps.

decay of the error, in our paper we change K_n by the following recursive formula:

$$K_{n+1} = \begin{cases} \max\left(\frac{1}{\alpha}K_n, K_{\min}\right) & \text{if } \|\Gamma_{n,m_0}^{\mathcal{G}} - \Phi[\Gamma_{n,m_0}^{\mathcal{G}}; \mathbf{D}^{\mathcal{G}}]\| < \|\Gamma_{n+1}^{\mathcal{G}} - \Phi[\Gamma_{n+1}^{\mathcal{G}}; \mathbf{D}^{\mathcal{G}}]\| \\ \min(\beta K_n, K_{\max}) & \text{otherwise} \end{cases} \quad (29)$$

where $\Gamma_{n,m_0}^{\mathcal{G}} = \Phi^{m_0(n)}[\Gamma_n^{\mathcal{G}}; \mathbf{D}^{\mathcal{G}}]$, $\alpha = 2$, and $\beta = 1.2$. For the MG-Picard method we use $K_0 = 10$, $K_{\min} = 5$, and $K_{\max} = 100$, and for the MG-MDIIS method we use $K_0 = 100$, $K_{\min} = 10$, and $K_{\max} = 100$. This allows us to smooth the decay of error and to reduce the total number of the iteration steps (see Figure 2, dashed line).

Usually iterative algorithms stop when the norm of the residue is less than some threshold. However, this method has its own disadvantages. The first one is that a small residue between two iteration steps does not necessarily imply a small distance from the current approximation to the exact solution. The second one is that a threshold is typically given in dimensionless values which have no physical meaning, and thus

one has no guidelines to choose an appropriate threshold. In the current work we use another criteria to stop iteration steps. Multigrid iteration stops on the n -th iteration step if the following condition is satisfied:

$$\|\Gamma_n - \Gamma_{n+m}\| < \epsilon_{\text{tres}} \quad (30)$$

where m is such, that

$$\|\Gamma_{n+m}^{\mathcal{G}} - \Gamma_{n+m+1}^{\mathcal{G}}\| < 0.01 \|\Gamma_n^{\mathcal{G}} - \Gamma_{n+1}^{\mathcal{G}}\| \quad (31)$$

We use such a condition because usually $\Gamma_{n+m}^{\mathcal{G}}$ is a good approximation of the exact solution. In this paper we use a norm based on the SFE calculations:

$$\|\Gamma_1^{\mathcal{G}} - \Gamma_2^{\mathcal{G}}\| = |\Delta G_{\text{KH}}(\Gamma_1) - \Delta G_{\text{KH}}(\Gamma_2)| \quad (32)$$

The SFE is calculated in the 3DRISM-KH approximation:⁵⁴

$$\Delta G_{\text{KH}}(\Gamma^{\mathcal{G}}) = \rho k_B T \sum_{\alpha}^{N_{\text{solvent}}} \int_{\mathbb{R}^3} \theta(-h_{\alpha}(\mathbf{r})) h_{\alpha}(\mathbf{r}) - \frac{1}{2} c_{\alpha}(\mathbf{r}) h_{\alpha}(\mathbf{r}) - c_{\alpha}(\mathbf{r}) d\mathbf{r} \quad (33)$$

where $\theta(\cdot)$ is the heaviside step function. Because of such definition, our threshold has well-defined physical meaning and is measured in energy units. In our work we use $\epsilon_{\text{tres}} = 0.001$ kcal/mol.

To make the calculations faster, in addition to the multigrid technique we use several grids with the same spacing but different buffers. We introduce a grid-enlargement operator $e[\cdot]$ which enlarges the buffer of a grid. We introduce an operator $E[\cdot]$ which extrapolates a solution $\Gamma^{\mathcal{G}}$ to a grid $[e[\mathcal{G}]]$.

$$E[\Gamma^{\mathcal{G}}] = \Gamma^{e[\mathcal{G}]} \quad (34)$$

Because functions $\gamma_{\alpha}(\mathbf{r})$ tend to zero when $|\mathbf{r}| \rightarrow \infty$, operator $E[\cdot]$ extrapolates functions by adding zeros at those parts of the grid $[e[\mathcal{G}]]$ which do not belong to the grid \mathcal{G} . The scheme of the iteration can be written in the following way:

$$\Gamma_0^{\mathcal{G}} \xrightarrow{\text{solve 3DRISM eqs}} \Gamma_*^{\mathcal{G}} \xrightarrow{E[\cdot]} \Gamma_0^{e[\mathcal{G}]} \xrightarrow{\text{solve 3DRISM eqs}} \Gamma_*^{e[\mathcal{G}]} \xrightarrow{E[\cdot]} \dots \quad (35)$$

We start from a zero approximation $\Gamma_0^{\mathcal{G}}$ on the grid \mathcal{G} with a small buffer and using the scheme eq 35 after several steps we obtain a solution on a grid with a large buffer.

COMPUTATION DETAILS

We performed 3DRISM calculations for infinitely diluted aqueous solutions of argon, methane, methanol, and dimethyl ether (DME). For the partial charges and Lennard-Jones (LJ) parameters of the solute molecules we used the OPLS-AA force-field parameters.⁵⁵ We used the MSPC-E water model⁴⁹ to describe solvent. In the 3DRISM calculations we used total site-site correlation functions of water which were initially calculated by the dielectrically consistent RISM technique.⁴⁹ Pairwise σ LJ parameters were calculated as an arithmetic mean of atomic parameters, pairwise ϵ LJ parameters were calculated as a geometric mean of atomic parameters:

$$\sigma_{12} = \frac{\sigma_1 + \sigma_2}{2}; \quad \epsilon_{12} = \sqrt{\epsilon_1 \cdot \epsilon_2} \quad (36)$$

Calculations were performed on the Intel(R) Xeon(R) CPU X5650 with the clocking 2.67 GHz. For calculation of the direct

and inverse fast Fourier transforms, the FFTW3 library was used.⁵⁶

RESULTS

Finding the Optimal Parameters for the Multigrid Solver. We performed 3DRISM calculations for infinitely diluted aqueous solutions of four compounds: argon, methane, methanol, and DME. To determine the optimal grid parameters, we performed SFE calculations on grids with different spacing parameters and different buffers. In Figure 3

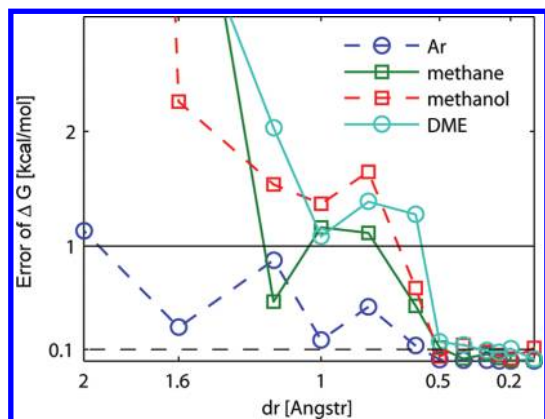


Figure 3. Dependency of the calculation errors on grid spacing at constant buffer (8 Å).

the dependence of calculation errors on the spacing parameter is shown. For the calculations we used several different grids with the fixed buffer of 8 Å and different spacings which vary from 0.1 to 2 Å. Errors were calculated as absolute values of the differences between SFEs calculated on a current grid and SFEs calculated on the very fine grid with the spacing of 0.05 and the buffer of 8 Å. The results show that the grid with the spacing of 0.2 Å provides an error that is less than 0.1 kcal/mol for all solutes, which is acceptable for the most of chemical applications. Thus in our work we use the grid with spacing of 0.2 Å.

In Figure 4 we show the dependency of calculation errors on the grid buffer. The calculations were performed on grids with fixed spacing of 0.2 Å and different buffers varying from 8 to 20 Å. Errors were calculated as differences between the SFEs

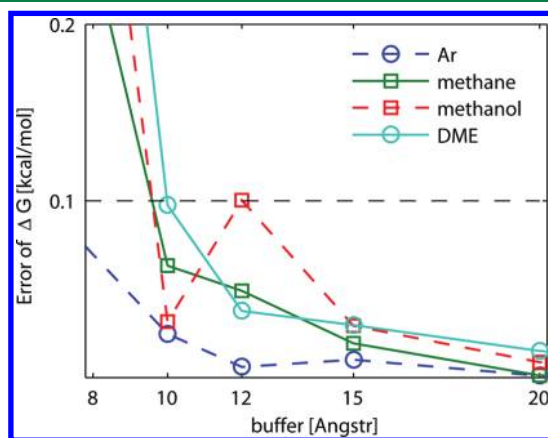


Figure 4. Dependency of calculation errors on the grid buffer with constant spacing of the grid (0.2 Å).

calculated on the current grid and the SFEs calculated on the very fine grid with spacing of 0.2 Å and buffer of 30 Å. The figure shows that the grid with the buffer of 15 Å is enough to provide the accuracy of SFE calculations ≤ 0.1 kcal/mol.

Computational Benchmarks of Different 3DRISM Solvers. To check the numerical performance of the proposed multigrid algorithm, we performed 3DRISM calculations for infinitely diluted aqueous solutions of argon, methane, methanol, and DME using the Picard iteration, the MDIIS, the MG-Picard, and the MG-MDIIS methods. For the Picard and the MDIIS methods, the grid with spacing of 0.2 Å and buffer of 15 Å was used. For the multigrid methods (MG-Picard, MG-DIIS), we used the scheme eq 35 with two enlargements: we started from the grid with the buffer of 7.65 Å, then moved to the grid with the buffer of 10.71 Å, and finished iteration on the grid with the buffer of 15 Å. Solutions on the grids with smaller buffers were used as initial guesses for the grids with larger buffers. For each buffer, we used the multigrid algorithm which uses 3 different grids (depth $l = 2$). All calculations were performed on the same personal computer, Intel(R) Xeon(R) CPU X5650 with clocking 2.67 GHz.

Computational expenses on solving 3DRISM equations for each of the investigated four methods are presented in Table 1.

Table 1. Computation Expenses of 3DRISM Calculations With the Picard Iteration, MDIIS, MG-Picard, and MG-MDIIS Methods

| compound | Picard iteration | MDIIS | MG-Picard | MG-DIIS |
|----------------|------------------|-------|-----------|---------|
| argon | 1148 s | 167 s | 46 s | 50 s |
| methane | 1484 s | 154 s | 149 s | 82 s |
| methanol | 1857 s | 416 s | 165 s | 83 s |
| dimethyl ether | 4462 s | 509 s | 241 s | 133 s |

These results show that the Picard iteration is the least efficient method, while the most efficient is the MG-MDIIS method. We note that the multigrid methods in all investigated cases are more efficient than the one-grid methods.

Figure 5 compares computational performance of the MDIIS, the MG-Picard, and the MG-MDIIS with the Picard

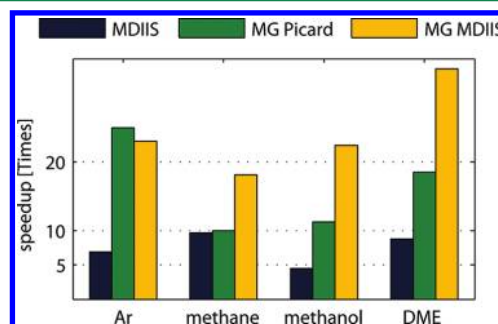


Figure 5. Speed up of the calculations by using the MDIIS, the MG-Picard and the MG-MDIIS methods as compared to the Picard iteration method.

iteration method. The figure shows that for all four compounds multigrid methods give more than 10 times speedup, while for three of these four compounds the MG-MDIIS method is more than 20 times faster than the Picard iteration method. Average speedup factors with respect to the plain Picard method for the MDIIS, the MG-Picard, and the MG-MDIIS methods are

correspondingly 7.4, 16.2, and 24.2. The most effective is the MG-MDIIS method that is on average about 3.5 faster than the MDIIS method. Difference between the multigrid methods is not very large: the MG-MDIIS method is in average only 1.5 times faster than the MG-Picard method. The results show that the multigrid scheme can be effectively used in combination with different types of coarse-grid iteration methods for solving the 3DRISM equations for aqueous solutions of small noncharged molecules.

Computational Benchmarks on a Large Set of Organic Molecules. The main goal of this part of our study was to investigate the overall efficiency of the new method in a view of large-scale practical applications like, e.g., physical-chemical profiling of large sets of organic compounds. We performed an additional benchmark and tested the efficiency of the new algorithm on a set of organic molecules as well as the accuracy of the SFE prediction. We estimate average computational expenses for the 3DRISM calculations also check whether numerical accuracy of the calculations is enough for accurate estimation of SFE.

We have chosen a set of 99 organic molecules. This set of molecules is a part of the set used in ref 21. The set includes alkanes, ketones, alkyl-benzenes, alcohols, alkyl-phenols, ethers, and other (polyfunctional) molecules. Quantity of atoms in molecules of the set varies from 5 to 31. Average number of atoms in a molecule is 16. The full list of molecules in the set is provided in the Supporting Information. The antechamber tool⁵⁷ from the Amber Tools 1.4 Package⁵⁸ was used for molecular structure optimization and assigning force field parameters. Structures of the molecules were optimized by using the AM1 method.⁵⁹ Atomic partial charges were calculated by using the bond charge correction (BCC) method.^{60,61} LJ parameters from the general Amber force field (GAFF)⁶² were assigned to the solutes. The benchmark calculations for simple molecules reported above show that the most effective is a combination of the multigrid and MDIIS(MG-MDIIS) methods. Therefore, we use the MG-MDIIS algorithm in our benchmarking of the overall efficiency of the method.

Figure 6 shows dependency of the computational time spent on MG-MDIIS 3DRISM calculations on the number of atoms in a molecule. The plot shows that the computational time can essentially vary for different molecules, even if the molecules have the same number of atoms. However, this somehow counterintuitive result has a straightforward explanation.

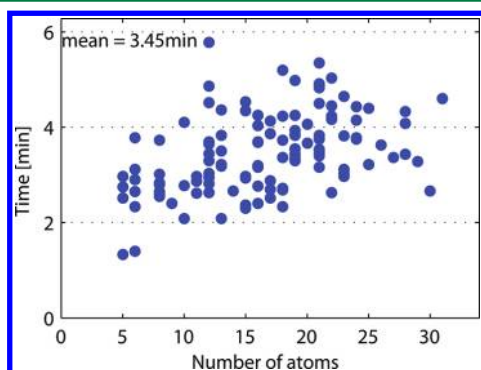


Figure 6. Dependency of the computational time spent on MG-MDIIS calculations on the molecule number of atoms for 99 organic molecules from the chosen molecule set.

Indeed, convergence of the algorithm depends not only on the number of atoms but also on the chemical composition of a molecule and its structure, particularly on the distribution of atomic partial charges and the molecule surface accessible area. This is illustrated by the results shown in Figures 3 and 4 that show different error dependencies for polar and nonpolar molecules. Also, even if two different molecules have the same number of atoms, they may still have rather different shapes. This can result in different grid sizes for them. More compact molecules need smaller grids than the less compact molecules, even if they have the same buffer and the same number of atoms. Therefore, combination of these two factors causes this significant deviation of computational time for molecules of the same number of atoms. However, the computational time for any molecule in the set is still less than 6 min. Average computational time is some 3.5 min (3 min 27 s).

We used the 3DRISM correlation functions calculated by MG-MDIIS method as an input for SFE calculations for all molecules from the above-mentioned set of 99 organic compounds. We used 25 molecules as a training set and the rest of the set (74 molecules) as a test set. The lists of all compounds in the training and test sets are given in the Supporting Information. For accurate SFE calculations, we used the universal correction (UC) method that was introduced in recent papers (refs 20 and 21). We tested two modifications of the UC method. The first one (UC-KH method) is based on the Kovalenko–Hirata (KH) free energy functional eq 33. The second one (UC-GF method) is based on the free energy calculations using the Gaussian fluctuations (GF) formula:⁶³

$$\Delta G_{\text{GF}} = \rho k_{\text{B}} T \sum_{\alpha=1}^{N_{\text{site}}} \int_{\mathbb{R}^3} \left(-\frac{1}{2} h_{\alpha}(\mathbf{r}) c_{\alpha}(\mathbf{r}) - c_{\alpha}(\mathbf{r}) \right) d\mathbf{r} \quad (37)$$

where k_{B} is the Boltzmann constant, T is the temperature, and ρ is the number density of a bulk solvent. In the UC-GF method ($\Delta G_{\text{UC}}^{\text{GF}}$) and in the UC-KH method ($\Delta G_{\text{UC}}^{\text{KH}}$), SFE is calculated by using the following relations:

$$\Delta G_{\text{UC}}^{\text{GF}} = \Delta G_{\text{GF}} + a_{\text{GF}} \rho V + b_{\text{GF}} \quad (38)$$

$$\Delta G_{\text{UC}}^{\text{KH}} = \Delta G_{\text{KH}} + a_{\text{KH}} \rho V + b_{\text{KH}} \quad (39)$$

where V is the partial molar volume of the molecule and a_{GF} , b_{GF} , a_{KH} , and b_{KH} are calculated by using the linear regression method to fit experimental data. Partial molar volume of a molecule was calculated by the following formula:^{64,65}

$$V = \left(\frac{1}{\rho} + 4\pi \int_0^{\infty} (g_{\text{oo}}(r) - 1) r^2 dr \right) \left(1 - \rho \sum_{\alpha=1}^{N_{\text{site}}} \int_{\mathbb{R}^3} c_{\alpha}(\mathbf{r}) d\mathbf{r} \right) \quad (40)$$

where $g_{\text{oo}}(r)$ is the oxygen–oxygen RDF of bulk water.

Using the training set of compounds, the following values of coefficients were obtained by the linear regression fitting procedure:^{11,21} $a_{\text{GF}} = -2.23$ kcal/mol and $b_{\text{GF}} = 1.28$ kcal/mol for the UC-GF method and $a_{\text{KH}} = -3.51$ kcal/mol and $b_{\text{KH}} = 0.81$ kcal/mol for the UC-KH. Figure 7a,b shows the correlation between the experimental values ΔG_{exp} and the calculated values $\Delta G_{\text{UC}}^{\text{GF}}$ and $\Delta G_{\text{UC}}^{\text{KH}}$. The correlation coefficient is 0.97 for the both methods. Root mean square deviation (rmsd) on a test set is 0.96 kcal/mol for the UC-GF method and 0.84 kcal/mol for the UC-KH method. Accuracy of

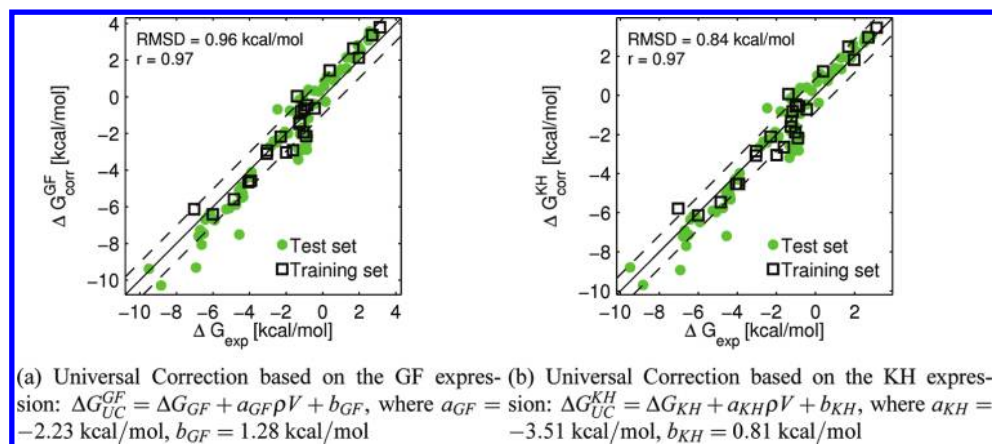


Figure 7. Correlation of experimentally measured SFEs with the SFEs values calculated by the UC method for the investigated set of organic molecules.

predictions is comparable with accuracies of experimental methods^{12,66} and corresponds to accuracies of current state-of-the-art methods for SFE calculations by molecular dynamics^{67–70} and other advanced molecular theories (e.g., energy representation method by Matubayasi and Nakahara, refs 71–73).^{9,74} Thus we show that the numerical accuracy of the algorithm is enough for SFE calculations and parametrization of calculation results.

CONCLUSIONS

In this paper, we proposed a new multigrid based method which solves the 3DRISM equations. To determine the optimal grid parameters, we performed 3DRISM calculations for infinitely diluted aqueous solutions of argon, methane, methanol, and dimethyl ether. We showed that on the grid with the spacing of 0.2 Å and the buffer of 15 Å, the maximal error is less than 0.1 kcal/mol. We tested two modifications of the multigrid algorithm: MG-Picard and MG-MDIIS methods. We compared the numerical efficiency of the multigrid algorithms with the numerical efficiency of the standard Picard iteration method and the MDIIS method. We showed that the MG-MDIIS algorithm is more than 24 times faster than the Picard iteration method and more than 3.5 times faster than the MDIIS method.

In turn, efficiencies of the MG-DIIS and MG-Picard methods do not differ very much. The MG-DIIS method is about 1.5 times faster than the MG-Picard method. We suggest that the most effective MG-MDIIS method can be used in the future as a fast tool for calculations of SFE for organic molecules. To support this statement, we performed 3DRISM calculations for aqueous solutions of 99 organic compounds. For all compounds in the set the computational time does not exceed 6 min per 1 molecule, while the average computational time is only 3.5 min per 1 molecule on a standard personal computer. We calculated SFEs by using GF and KH expressions with the universal partial molar volume corrections (UC-GF and UC-KH methods). We showed that calculated and experimental values of solvation free energy are strongly correlated to each other (correlation coefficient is 0.97). Rmsd error for the test set of compounds is less than 1 kcal/mol for both UC-GF and UC-KH methods. The performed tests show that the proposed algorithm can be used for fast and accurate predictions of aqueous solvation free energies of neutral molecules.

ASSOCIATED CONTENT

Supporting Information

The list of the organic molecules used in the paper for benchmarking of the algorithm and for the dependencies of the computational time on the λ and η parameters. This material is available free of charge via the Internet at <http://pubs.acs.org>.

AUTHOR INFORMATION

Corresponding Author

*E-mail: maxim.fedorov@strath.ac.uk. Telephone: +44 (0)141-5484012.

Notes

The authors declare no competing financial interest.

ACKNOWLEDGMENTS

We are grateful to Wolfgang Hackbusch for insightful discussions on different aspects of multigrid mathematical background. We thank David S. Palmer for critical reading of the manuscript. This work was partially supported by Deutsche Forschungsgemeinschaft (DFG) - German Research Foundation, research grant FE 1156/2-1 and REA Research Executive Agency, grant no. 247500 “BioSol”, Programme: FP7-PEOPLE-2009-IRSES.

REFERENCES

- (1) Ornstein, L. S.; Zernike, F. *Proc. K. Ned. Akad. Wet.* **1914**, *17*, 793–806.
- (2) Hansen, J.-P.; McDonald, I. R. *Theory of Simple Liquids*, 4th ed; Elsevier Academic Press: Amsterdam, The Netherlands, 2000.
- (3) Chandler, D.; Andersen, H. C. *J. Chem. Phys.* **1972**, *57*, 1930–1937.
- (4) Ten-no, S.; Hirata, F.; Kato, S. *Chem. Phys. Lett.* **1993**, *214*, 391–396.
- (5) Sato, H.; Hirata, F.; Kato, S. *J. Chem. Phys.* **1996**, *105*, 1546–1551.
- (6) Yokogawa, D.; Sato, H.; Sakaki, S. *J. Chem. Phys.* **2007**, *126*, 244504.
- (7) Singer, S. J.; Chandler, D. *Mol. Phys.* **1985**, *55*, 621–625.
- (8) Ten-no, S. *J. Chem. Phys.* **2001**, *115*, 3724–3731.
- (9) Karino, Y.; Fedorov, M. V.; Matubayasi, N. *Chem. Phys. Lett.* **2010**, *496*, 351–355.
- (10) Palmer, D. S.; Sergiievskiy, V. P.; Jensen, F.; Fedorov, M. V. *J. Chem. Phys.* **2010**, *133*, 044104.
- (11) Ratkova, E. L.; Chuev, G. N.; Sergiievskiy, V. P.; Fedorov, M. V. *J. Phys. Chem. B* **2010**, *114*, 12068–12079.

- (12) Ratkova, E. L.; Fedorov, M. V. *J. Chem. Theory Comput.* **2011**, *7*, 1450–1457.
- (13) Sergiievskiy, V. P. *Russ. J. Phys. Chem. B* **2011**, *5*, 326–331.
- (14) Chandler, D.; McCoy, J. D.; Singer, S. J. *J. Chem. Phys.* **1986**, *85*, 5971–5976.
- (15) Beglov, D.; Roux, B. *J. Chem. Phys.* **1995**, *103*, 360–364.
- (16) Imai, T. *Condens. Matter Phys.* **2007**, *10*, 343–361.
- (17) Yokogawa, D.; Sato, H.; Imai, T.; Sakaki, S. *J. Chem. Phys.* **2009**, *130*, 064111.
- (18) Luchko, T.; Gusarov, S.; Roe, D. R.; Simmerling, C.; Case, D. A.; Tuszynski, J.; Kovalenko, A. *J. Chem. Theory Comput.* **2010**, *6*, 607–624.
- (19) Stumpe, M. C.; Blinov, N.; Wishart, D.; Kovalenko, A.; Pande, V. S. *J. Phys. Chem. B* **2011**, *115*, 319–328.
- (20) Palmer, D. S.; Chuev, G. N.; Ratkova, E. L.; Fedorov, M. V. *Curr. Pharm. Des.* **2011**, *17*, 1695–1708.
- (21) Frolov, A. I.; Ratkova, E. L.; Palmer, D. S.; Fedorov, M. V. *J. Phys. Chem. B* **2011**, *115*, 6011–6022.
- (22) Monson, P. A.; Morriss, G. P. *Adv. Chem. Phys.* **1990**, *77*, 451–550.
- (23) Zerah, G. *J. Comput. Phys.* **1985**, *61*, 280–285.
- (24) Booth, M. J.; Schlijper, A.; Scales, L.; Haymet, A. *Comput. Phys. Commun.* **1999**, *119*, 122–134.
- (25) Kawata, M.; Cortis, C. M.; Friesner, R. A. *J. Chem. Phys.* **1998**, *108*, 4426–4438.
- (26) Kovalenko, A.; Ten-No, S.; Hirata, F. *J. Comput. Chem.* **1999**, *20*, 928–936.
- (27) Homeier, H.; Rast, S.; Krienke, H. *Comput. Phys. Commun.* **1995**, *92*, 188–202.
- (28) Gillan, M. J. *Mol. Phys.* **1979**, *38*, 1781–1794.
- (29) Labik, S.; Malijevsky, A.; Vonka, P. *Mol. Phys.* **1985**, *56*, 709–715.
- (30) Woelki, S.; Kohler, H.; Krienke, H.; Schmeer, G. *Phys. Chem. Chem. Phys.* **2008**, *10*, 898–910.
- (31) Chuev, G. N.; Fedorov, M. V. *J. Comput. Chem.* **2004**, *25*, 1369–1377.
- (32) Chuev, G. N.; Fedorov, M. V. *J. Chem. Phys.* **2004**, *120*, 1191–1196.
- (33) Fedorov, M. V.; Chuev, G. N. *J. Mol. Liq.* **2005**, *120*, 159–162.
- (34) Fedorov, M. V.; Flad, H. J.; Chuev, G. N.; Grasedyck, L.; Khoromskij, B. N. *Computing* **2007**, *80*, 47–73.
- (35) Hackbusch, W. *Multi-grid methods and Applications*; Springer-Verlag: Berlin, Germany, 1985.
- (36) Wang, H. Y.; Jiang, W.; Wang, Y. N. *Plasma Sources Sci. Technol.* **2010**, *19*, 045023.
- (37) Heiskanen, M.; Torsti, T.; Puska, M.; Nieminen, R. *Phys. Rev. B* **2001**, *63*, 245106.
- (38) Janke, W.; Sauer, T. *Phys. Rev. E* **1994**, *49*, 3475–3479.
- (39) Gygi, F.; Galli, G. *Phys. Rev. B* **1995**, *52*, R2229–R2232.
- (40) Kelley, C. T.; Pettitt, B. M. *J. Comput. Phys.* **2004**, *197*, 491–501.
- (41) Marucho, M.; Kelley, C. T.; Pettitt, B. M. *J. Chem. Theory Comput.* **2008**, *4*, 385–396.
- (42) Sergiievskiy, V. P.; Hackbusch, W.; Fedorov, M. V. *J. Comput. Chem.* **2011**, *32*, 1982–1992.
- (43) Kovalenko, A.; Hirata, F. *Chem. Phys. Lett.* **1998**, *290*, 237–244.
- (44) Kovalenko, A.; Hirata, F. *J. Chem. Phys.* **2000**, *112*, 10403–10417.
- (45) Kovalenko, A.; Truong, T. N. *J. Chem. Phys.* **2000**, *113*, 7458–7470.
- (46) Kovalenko, A.; Hirata, F. *J. Chem. Phys.* **2000**, *113*, 2793–2805.
- (47) Harano, Y.; Imai, T.; Kovalenko, A.; Kinoshita, M.; Hirata, F. *J. Chem. Phys.* **2001**, *114*, 9506–9511.
- (48) Kovalenko, A.; Hirata, F. *J. Phys. Chem. B* **1999**, *103*, 7942–7957.
- (49) Fedorov, M. V.; Kornyshev, A. A. *Mol. Phys.* **2007**, *105*, 1–16.
- (50) Perkyns, J. S.; Lynch, G. C.; Howard, J. J.; Pettitt, B. M. *J. Chem. Phys.* **2010**, *132*, 064106.
- (51) Ng, K. C. *J. Chem. Phys.* **1974**, *61*, 2680–2689.
- (52) Kovalenko, A.; Hirata, F. *J. Chem. Phys.* **1999**, *110*, 10095–10112.
- (53) Pulay, P. *Chem. Phys. Lett.* **1980**, *73*, 393–398.
- (54) *Molecular theory of solvation*; Hirata, F., Ed.; Kluwer Academic Publishers: Dordrecht, The Netherlands, 2003.
- (55) Jorgensen, W. L.; Maxwell, D. S.; Tirado-Rives, J. *J. Am. Chem. Soc.* **1996**, *118*, 11225–11236.
- (56) Frigo, M. *ACM SIGPLAN Notices* **1999**, *34*, 169–180.
- (57) Wang, J. M.; Wang, W.; Kollman, P. A.; Case, D. A. *J. Mol. Graphics Modell.* **2006**, *25*, 247–260.
- (58) Case, D. A.; Cheatham, T. E.; Darden, T.; Gohlke, H.; Luo, R.; Merz, K. M.; Onufriev, A.; Simmerling, C.; Wang, B.; Woods, R. J. *J. Comput. Chem.* **2005**, *26*, 1668–1688.
- (59) Dewar, M. J. S.; Zoebisch, E. G.; Healy, E. F.; Stewart, J. J. P. *J. Am. Chem. Soc.* **1985**, *107*, 3902–3909.
- (60) Jakalian, A.; Bush, B. L.; Jack, D. B.; Bayly, C. I. *J. Comput. Chem.* **2000**, *21*, 132–146.
- (61) Jakalian, A.; Jack, D. B.; Bayly, C. I. *J. Comput. Chem.* **2002**, *23*, 1623–1641.
- (62) Wang, J. M.; Wolf, R. M.; Caldwell, J. W.; Kollman, P. A.; Case, D. A. *J. Comput. Chem.* **2004**, *25*, 1157–1174.
- (63) Chandler, D.; Singh, Y.; Richardson, D. M. *J. Chem. Phys.* **1984**, *81*, 1975–1982.
- (64) Imai, T.; Kinoshita, M.; Hirata, F. *Bull. Chem. Soc. Jpn.* **2000**, *73*, 1113–1122.
- (65) Imai, T.; Harano, Y.; Kovalenko, A.; Hirata, F. *Biopolymers* **2001**, *59*, 512–519.
- (66) Guthrie, J. P. *J. Phys. Chem. B* **2009**, *113*, 4501–4507.
- (67) Udier-Blagovic, M.; De Tirado, P. M.; Pearlman, S. A.; Jorgensen, W. L. *J. Comput. Chem.* **2004**, *25*, 1322–1332.
- (68) Shirts, M. R.; Pande, V. S. *J. Chem. Phys.* **2005**, *122*, 134508.
- (69) Shivakumar, D.; Williams, J.; Wu, Y. J.; Damm, W.; Shelley, J.; Sherman, W. *J. Chem. Theory Comput.* **2010**, *6*, 1509–1519.
- (70) Paluch, A. S.; Shah, J. K.; Maginn, E. J. *J. Chem. Theory Comput.* **2011**, *7*, 1394–1403.
- (71) Matubayasi, N.; Nakahara, M. *J. Chem. Phys.* **2000**, *113*, 6070–6081.
- (72) Matubayasi, N.; Nakahara, M. *J. Chem. Phys.* **2002**, *117*, 3605–3616.
- (73) Matubayasi, N.; Nakahara, M. *J. Chem. Phys.* **2003**, *119*, 9686–9702.
- (74) Matubayasi, N. *Front. Biosci.* **2009**, *14*, 3536–3549.